ADVANCED ENERGY MATERIALS

www.advenergymat.de

An Interconnected Channel-Like Framework as Host for Lithium Metal Composite Anodes

*Hansen Wang, Dingchang Lin, Jin Xie, Yayuan Liu, Hao Chen, Yanbin Li, Jinwei Xu, Guangmin Zhou, Zewen Zhang, Allen Pei, Yangying Zhu, Kai Liu, Kecheng Wang, and Yi Cui**

Lithium (Li) metal anodes have long been counted on to meet the increasing demand for high energy, high-power rechargeable battery systems but they have been plagued by uncontrollable plating, unstable solid electrolyte interphase (SEI) formation, and the resulting low Coulombic efficiency. These problems are even aggravated under commercial levels of current density and areal capacity testing conditions. In this work, the channel-like structure of a carbonized eggplant (EP) as a stable "host" for Li metal melt infusion, is utilized. With further interphase modification of lithium fluoride (LiF), the as-formed EP–LiF composite anode maintains ≈90% Li metal theoretical capacity and can successfully suppress dendrite growth and volume fluctuation during cycling. EP–LiF offers much improved symmetric cell and full-cell cycling performance with lower and more stable overpotential under various areal capacity and elevated rate capability. Furthermore, carbonized EP serves as a lightweight high-performance current collector, achieving an average Coulombic efficiency ≈99.1% in ether-based electrolytes with 2.2 mAh cm^{-2} cycling areal capacity. The natural structure of carbonized EP will inspire further artificial designs of electrode frameworks for both Li anode and sulfur cathodes, enabling promising candidates for next-generation high-energy density batteries.

Rechargeable lithium (Li)-ion batteries dominate current portable electronics and electric vehicles markets.[1] However, traditional graphite anodes and Li metal oxide cathodes have fallen behind the increasing needs for high-energy density energy storage systems.[2,3] New generation of anodes such as silicon, cathodes such as sulfur and oxygen has been considered.[4] Particularly, with nanomaterials design, the challenging problems associated with these materials have been addressed with exciting progress.[5] Li metal has been considered as the "Holy Grail" of battery chemistry due to its highest specific capacity (3860 mAh g^{-1}) and lowest potential (–3.04 V vs standard hydrogen electrode). These properties endow Li metal with the potential of becoming the ultimate anode material for a battery. However, massive efforts are still needed to solve the critical issues of Li metal. The problems of Li metal roots from its "hostless" nature and high chemical reactivity.[3] It is known that Li metal will spontaneously react with organic electrolytes, forming a solid electrolyte interphase (SEI). Ideally, if this SEI layer is chemically stable and mechanically strong, it can prevent Li metal from further exposure to electrolytes. However, the "hostless" Li metal anode experiences infinite relative volume change during charging and discharging. This huge volume change will crack the SEI and continuously expose fresh Li metal to electrolytes and consume the active material. Worse still, the increased ion flux will lead Li metal to be preferentially plated at the cracks, causing dendritic Li metal growth. Li dendrites will not only trigger possible safety issue (short circuit), but also greatly increase surface area and give rise to the formation of electrochemically inactive "dead Li." As a result, the capacity of Li metal anodes decays too fast to be used in practical batteries.

To deal with this "hostless" nature of Li metal, we proposed the idea of artificial "host" recently. Various 3D porous frameworks, including reduced graphene oxide thin film,[6] polymer fiber matrix,[7] amorphous carbon spheres,[8] carbon fiber film,[9,10] over-lithiated oxide, and fluoride matrix[11,12] were fabricated as reservoirs for Li metal. Li metal can be stored into these frameworks through electrochemical deposition, melt infusion, or high temperature reaction. As a result, the electrode volume can be maintained with little change during cycling, leading to a much more stable SEI, homogeneous Li metal deposition, and higher Coulombic efficiency. However, a "host" structure alone does not seem to be enough for solving all the problems related to Li metal. In most cases, the "host" structures are porous and still open to the electrolytes. A small disturbance will break the SEI and lead to Li metal loss. So much efforts have also been made to improve the quality of SEI. Some works change the electrolyte recipe to form a better SEI,[13–20] others directly fabricate artificial SEI onto Li foil with properties beneficial to Li metal cycling.[21–28] These novel SEIs

H. Wang, D. Lin, Dr. J. Xie, Y. Liu, Dr. H. Chen, Y. Li, J. Xu, Dr. G. Zhou, Z. Zhang, A. Pei, Dr. Y. Zhu, Dr. K. Liu, Dr. K. Wang, Prof. Y. Cui
Department of Materials Science and Engineering
Stanford University
Stanford, CA 94305, USA
E-mail: yicui@stanford.edu
Prof. Y. Cui
Stanford Institute for Materials and Energy Sciences
SLAC National Accelerator Laboratory
2575 Sand Hill Road, Menlo Park, CA 94025, USA

The ORCID identification number(s) for the author(s) of this article can be found under https://doi.org/10.1002/aenm.201802720.

DOI: 10.1002/aenm.201802720

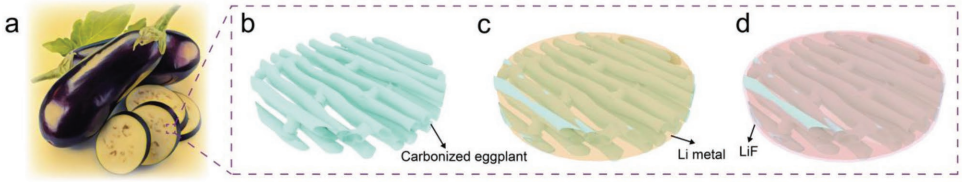

Figure 1. a) Photo of an eggplant and its cross-section morphology. b) Schematic illustration for a carbonized EP with interconnected channel-like structure. c) Carbonized EP after Li metal melt infusion. d) Carbonized EP–Li metal composite anode further coated with a layer of LiF thin film.

usually have higher mechanical strength and can promote homogenous Li metal plating. Nevertheless, achieving high enough Coulombic efficiency still remains as a road block for the advancement of Li metal research.

From the discussion above, further engineering the SEI of a 3D Li metal composite anode will be crucial to combining the volume maintaining capability with a good interphase and boosting the cycling efficiency. Herein, we propose a novel design of a lithium fluoride (LiF)-coated carbonized eggplant-Li metal composite anode (EP–LiF) to address all the issues above. EP has long been found to have a channel-like structure in its endocarp,[29] which is the main component of the fruit. This interconnected channel structure not only enables high surface area[30,31] as frameworks for supercapacitors[31–33] and catalysts,[30] but also guarantees its potential for uniform Li melt infiltration and fast electron and ion transportation serving as a 3D host material in the battery field. Attributed to the high porosity and low density of carbonized EP, EP–LiF possesses the highest specific capacity (3461 mAh g^{-1}) among all the Li metal composite anodes reported so far. Meanwhile, surface of the composite anode is protected by a dual strategy. On one hand, LiF coating outside the composite anode promotes Li diffusion at the interphase, suppressing dendritic growth.[34–42] On the other hand, graphitic nature of the carbonized EP framework further stabilizes SEI, benefiting Li nucleation and leading to a higher Coulombic efficiency. As a result of these features, this interphase-protected 3D composite Li anode successfully suppressed volume fluctuation and dendrite growth during cycling, enabling highly improved electrochemical performance in both half cells and full cells. With its low cost, simple synthesis procedure, EP–LiF may possibly serve as a scalable Li metal anode for next-generation high-energy density batteries systems.

Figures 1 and **2** illustrate the fabrication process of EP–LiF. A fresh EP (Figure 1a) was first frozen and dried to get rid of all the water in the structure without shrinkage. Then the dry EP was cut into thin pieces and punched into round shape (Figure 2a, inset). The interconnected channel-like structures

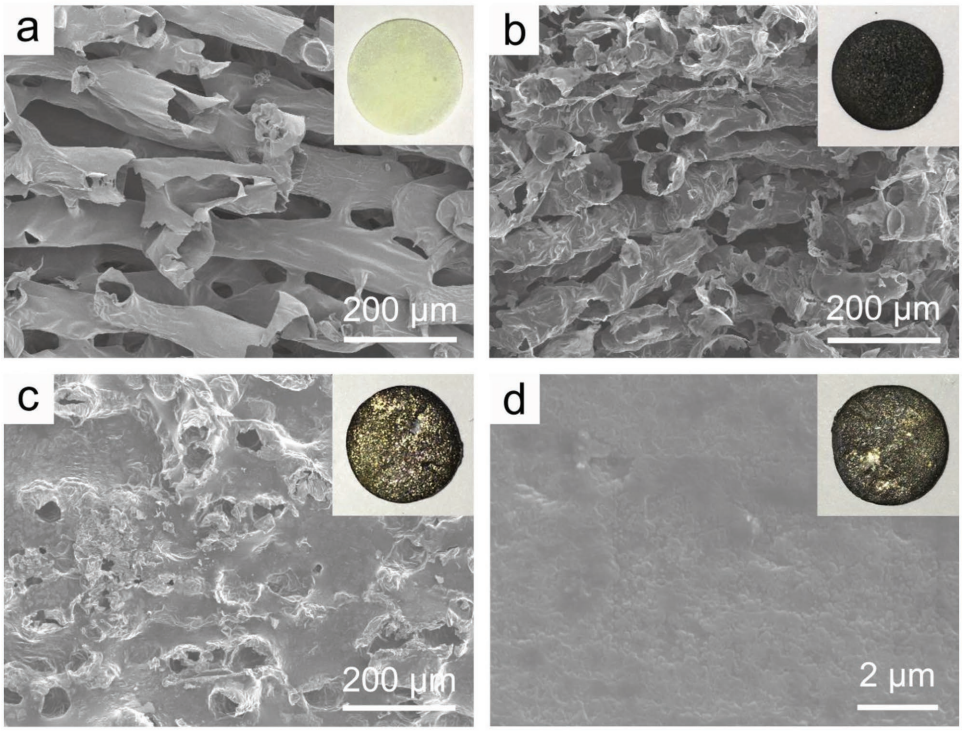

Figure 2. a) SEM image and digital photo (inset) of a piece of freeze-dried EP. b) SEM image and digital photo (inset) of a piece of carbonized EP. c) SEM image and digital photo (inset) of a piece of carbonized EP after Li metal infusion. d) SEM image and digital photo (inset) of a piece of EP–LiF composite anode.

can be clearly observed under scanning electron microscopy (SEM) (Figure 2a). Then the freeze-dried EP was carbonized under 1000 °C and Ar atmosphere for 4 h to form carbonized EP. The channel-like structure could be maintained after carbonization (Figure 2b) and the color of the EP sample turned to black (Figure 2b, inset). This structure is also schematically illustrated in Figure 1b. Energy-dispersive X-ray spectroscopy (EDS) and X-ray photoelectron spectroscopy (XPS) results confirm that the carbonized EP is composed of carbon framework with tiny amount of mineral salt precipitants (Figures S1, S2, Supporting Information). N_2 adsorption–desorption isotherm (Figure S3, Supporting Information) shows that carbonized EP has a large surface area of 1174.2 m^2 g^{-1}, indicating its ability to accommodate large quantity of Li metal for a high specific capacity as well as to reduce local current density for fast charging/discharging. Subsequently a piece of carbonized EP was coated with zinc oxide (ZnO) using atomic layer deposition (ALD) to functionalize its surface to be lithiophilic.[7] With a melt infusion process, Li metal was heated up to around 350 °C, and a piece of ZnO-coated carbonized EP was placed onto the Li metal melt. Li metal would infuse into the interconnected channels of carbonized EP due to capillary force, forming a carbonized EP/Li metal composite anode (Figures 1c and 2c). It can be observed that the carbonized EP became shinny (Figure 2c, inset), proving the infiltration of Li metal. Finally, the composite anode was coated with a layer of LiF through the reaction with gaseous reagent Freon under 0.5 atm and 120 °C for 24 h to get EP–LiF anode (Figure 1d). The specific process for LiF coating has been reported previously.[22] With the LiF coating, the EP–LiF surface was obscurer with a little bit of purple in color (Figure 2d, inset). High magnification SEM (Figure 2d) shows the morphology of EP–LiF. LiF layer coated onto Li foil under same condition was illustrated to have high uniformity under tens of microns scale (Figure S4, Supporting Information). XPS depth profile of Li 1s and F 1s further demonstrate the LiF coating properties (Figure S5, Supporting Information). After multiple sputtering, the signal of F 1s drops gradually, indicating the reduced thickness of LiF layer (Figure S5a, Supporting Information). Li 1s peak matches F 1s as well. Li 1s signal is fixed at ≈58.5 eV at early stages, corresponding to Li species in LiF. After multiple sputtering sessions, the peak moves to ≈56.5 eV, originated from the metallic Li under the LiF coating (Figure S5b, Supporting Information). According to previously sputtering–thickness relationship for LiF, the thickness of the coating onto EP–LiF can be estimated to be around 20–30 nm. Due to the high porosity and low density of carbon framework, EP–LiF was able to maintain a high specific capacity of 3461 mAh g^{-1} (including the weight of Li metal and carbon) after being charged to 1 V versus Li/Li^+ under 50 μA cm^{-2} current density (Figure S6, Supporting Information). This is around 90% of the theoretical specific capacity of Li metal (3860 mAh g^{-1}), meaning that the "host" structure does not really diminish the advantage of high capacity for Li metal. Such low occupation of "host" structure provides EP–LiF with much higher specific capacity compared to previous host structures,[7,10,11] including previously used rGO framework,[6] offering exciting possibilities for highly rechargeable Li metal fabrication methods without compromising its capacity.

Later, Li metal morphology after cycling in a symmetric cell setup was observed under SEM. **Figure 3**a shows the top-view image of an EP–LiF electrode after one symmetric cell cycle with current density of 1 mA cm^{-2} and areal capacity of 1 mAh cm^{-2}, while Figure 3c shows that of a Li foil. Dendritic growth could be clearly observed for bare Li foil. Li metal filaments with diameter from 200 nm to 2 μm tangled together, increasing Li metal exposure area to the electrolyte and aggravating Li metal capacity decay. On the contrary, EP–LiF was able to achieve a rather homogeneous Li metal deposition morphology. The grain boundary on the EP–LiF anode surface confirmed that the observed Li metal was indeed freshly plated with high homogeneity instead of the initial infused Li metal. Li metal plating morphology after longer cycling was also characterized. Figure 3b shows the top-view image of an EP–LiF anode after 10 symmetric cell cycles under 1 mA cm^{-2} and 1 mAh cm^{-2}, while Figure 3d shows that of a Li foil. Li metal dendrites on bare Li foil became thinner. This is because the continuous cycling created much dead Li and also SEI shells from previous cycling. The thinner Li metal dendrites not only exacerbated fresh Li metal consumption, but also would increase the possibility of short circuit and severe battery thermal runaway. As for EP–LiF, although the surface was roughened slightly, the plated Li metal still maintained an intact piece without much increased surface area. After 100 cycles under 1 mA cm^{-2} and 1 mAh cm^{-2}, EP–LiF was still able to maintain a rather uniform morphology, which is further demonstrated in Figure S7b in the Supporting Information. Li dendrite was successfully suppressed mainly because of two reasons. Firstly, the "host" structure of carbonized EP reduced the possibility of SEI cracking during cycling, thus increasing Li ion flux homogeneity among the interphase and better Li plating morphology. Secondly, the function of LiF for suppressing dendritic growth has been previously reported. LiF is able to lower the Li diffusion activation energy barrier at the electrolyte/Li interphase, leading to an increased Li diffusivity by more than two orders of magnitude.[20] As a result, Li metal tends to be deposited laterally into smooth surface instead of horizontally into dendrites.[10,23] This effect of LiF can be illustrated through Figure S7a in the Supporting Information, where the surface of an EP–Li composite anode without LiF protection after 100 cycles under 1 mA cm^{-2} and 1 mAh cm^{-2} was much messier compared to that with LiF protection.

Electrochemical impedance spectroscopy (EIS) was tested for Li foil and EP–LiF symmetric cells after various numbers of cycles and the results matched the SEM characterizations pretty well. It is well known that Li foil symmetric cell will experience a large resistance decrease (diameter of semicircles in Figure S8 in the Supporting Information) after cycling due to the significant increase in actual surface area after dendrite growth. Our impedance data (Figure S8b, Supporting Information) confirmed that the impedance of a Li foil symmetric cell fell from about 1500 to 40 Ω cm^2 after 20 cycles under 1 mA cm^{-2} and 1 mAh cm^{-2}. As for EP–LiF symmetric cells (Figure S8a, Supporting Information), the initial impedance (≈80 Ω cm^2) was much smaller than that of Li foil cells, attributed to the modified SEI composition and the increased electrochemical surface area. After 20 cycles, the impedance of EP–LiF remained largely unchanged, which further confirmed the smooth surface after

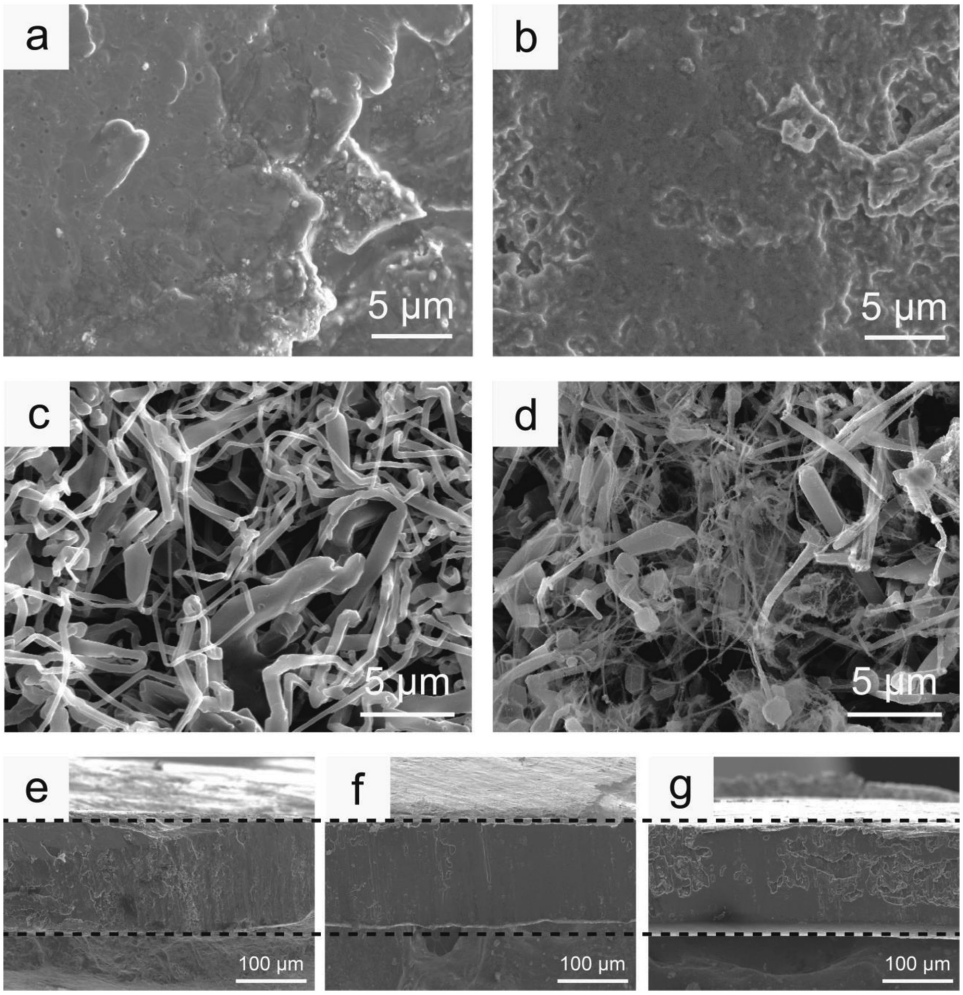

Figure 3. Top-view SEM image of EP–LiF anode after a) 1 cycle and b) 10 cycles under 1 mA cm^{-2} and 1 mAh cm^{-2} in a symmetric cell. Top-view SEM image of Li foil anode after c) 1 cycle and d) 10 cycles under 1 mA cm^{-2} and 1 mAh cm^{-2} in a symmetric cell. Cross-section of e) a pristine EP–LiF electrode, f) an EP–LiF electrode after stripping ≈10 mAh cm^{-2} of capacity and g) an EP–LiF electrode after stripping ≈10 mAh cm^{-2} of capacity and plate it back.

cycling with no dendrites and actual surface area increase. As cycle number increased, the impedance of EP–LiF started to decrease to lower than 20 Ω cm^2. This was even lower than that of Li foil with lots of dendrites and high interphase area, indicating a much improved long-term cycling performance which we will show in later parts. We attribute the decrease in impedance to the reconstruction of SEI. As cycling proceeded, high Li ionic conductivity species will possibly be formed onto the EP–LiF electrolyte interphase, further reducing the resistance of the SEI layer.

Volume stability of EP–LiF anode was also characterized. In a typical experiment, an EP–LiF anode with thickness around 180 μm was evenly cut into three pieces. One of them was stripped of 10 mAh cm^{-2} Li metal, and another one was stripped of 10 mAh cm^{-2} capacity and then plated the same amount of Li back. Then the cross-section images of these three pieces EP–LiF electrodes were characterized under SEM (Figure 3e–g). It can be observed the thickness of EP–LiF electrode was maintained pretty well after Li metal stripping and plating back, confirming the capability of carbonized EP framework to prevent huge volume change during cycling, and also indicating a better electrochemical performance in symmetric and full cells.

Galvanostatic symmetric cell cycling under various conditions was characterized for EP–LiF and Li foil, respectively, in carbonate-based electrolyte. Figure S9 in the Supporting Information shows the voltage profile of EP–LiF and Li foil symmetric cells being cycled under current density of 1 mA cm^{-2} and capacity of 1 mAh cm^{-2}. Li foil symmetric cell showed a consistent high overpotential of about 100 mV, attributed to its low surface area. After 100 cycles, overpotential of Li foil cell started to increase due to the progressive SEI buildup and finally led to failure of the cell. As for EP–LiF, the initial overpotential was comparable to that of Li metal despite much increased surface area, due to the relatively low ionic conductivity of LiF. However, as SEI reconstruction happened, EP–LiF started to show lower overpotential around only 30 mV, and could be stably cycled for at least 600 cycles without fluctuation in the voltage plateau. Later, symmetric cell cycling tests were carried out at higher current densities of 3 mA cm^{-2}

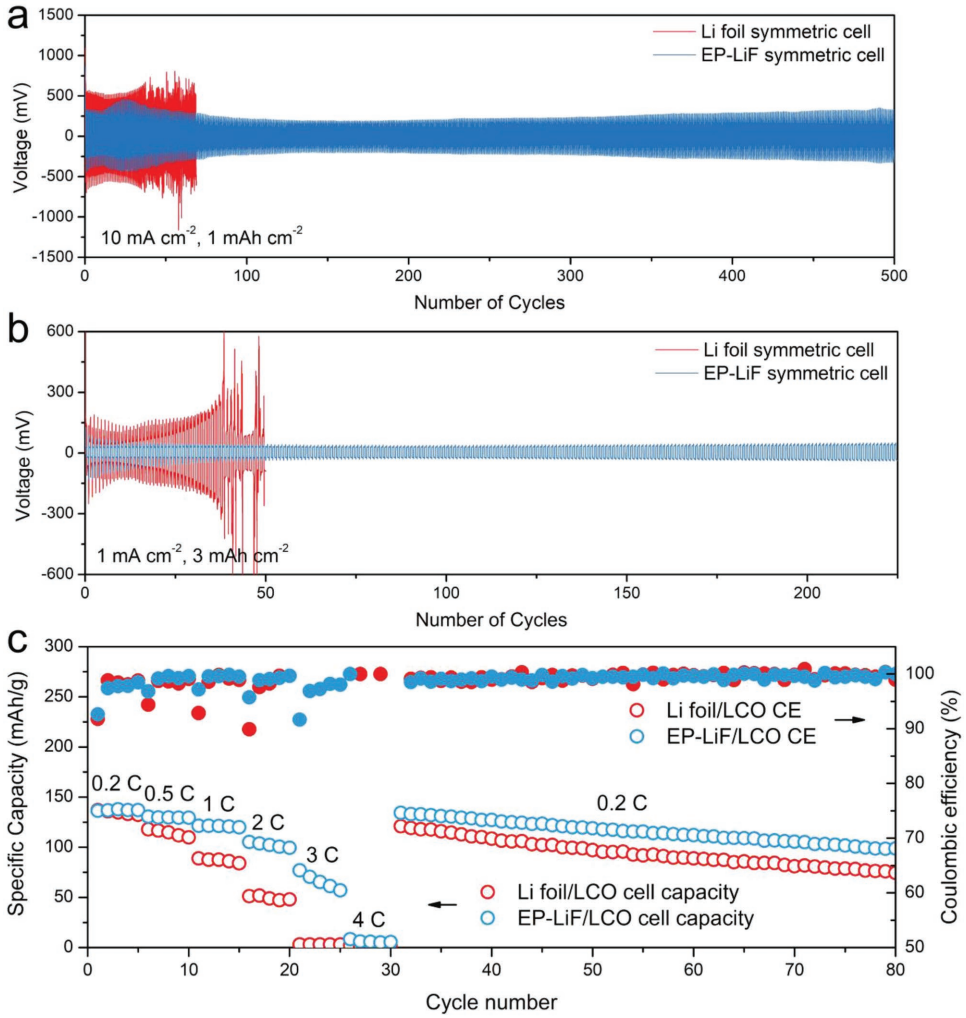

Figure 4. Symmetric cell cycling performance comparison between Li foil and EP–LiF under a) 10 mA cm^{-2}, 1 mAh cm^{-2} and b) 1 mA cm^{-2}, 3 mAh cm^{-2}. c) Rate capability comparison between Li foil/LCO full cell and EP–LiF/LCO full cell under various rates from 0.2 to 4 C.

(Figure S10, Supporting Information), 5 mA cm^{-2} (Figure S11, Supporting Information), and 10 mA cm^{-2} with areal capacity fixed at 1 mAh cm^{-2} (**Figure 4**a) for Li foil and EP–LiF. EP–LiF symmetric cell showed a consistent low overpotential of ≈90 mV under 3 mA cm^{-2}, ≈150 mV under 5 mA cm^{-2}, and ≈250 mV under 10 mA cm^{-2} after stabilization, while the overpotential for Li foil cell was high and fluctuating. Finally, we also tested symmetric cell cycling performance under higher areal capacity of 3 mAh cm^{-2} (Figure 4b) and 5 mAh cm^{-2} (Figure S12, Supporting Information) with current density fixed at 1 mA cm^{-2} for Li foil and EP–LiF. Li foil showed much larger overpotential especially at the end of each stripping and plating process, which can be attributed to the difficulty of utilizing the previously unused fresh Li metal below the poorly conducting SEI layer. And it can be barely cycled under 5 mAh cm^{-2} areal capacity. In comparison, EP–LiF symmetric cell showed much improved cycling performance with smooth voltage plateau and reduced overpotential after stabilization for at least 250 cycles under 3 mAh cm^{-2} and 150 cycles under 5 mAh cm^{-2}. These results indicate potential of EP–LiF for commercial level of cycling capability.

For full cell setup, Li foil and EP–LiF were firstly paired with lithium cobalt oxide (LCO) cathodes with areal mass loading of ≈7 mg cm^{-2} in carbonate-based electrolyte. EP–LiF/LCO full cell showed a much improved rate capability comparing to bare Li foil. At a low rate of 0.2 C, EP–LiF/LCO full cell was able to offer a consistent cycling specific capacity of ≈138 mAh g^{-1} (based on LCO mass), while Li foil/LCO could provide a comparable capacity but immediately started to decay afterwards (Figure 4c). Under higher rates, EP–LiF/LCO cell was capable to provide a specific capacity of ≈131 mAh g^{-1} under 0.5 C, ≈120 mAh g^{-1} under 1 C, ≈105 mAh g^{-1} under 2 C, ≈70 mAh g^{-1} under 3 C, and finally ≈10 mAh g^{-1} under 4 C. In comparison, Li foil/LCO full cell showed specific capacity of ≈115 mAh g^{-1} under 0.5 C, ≈90 mAh g^{-1} under 1 C, ≈50 mAh g^{-1} under 2 C with consistent capacity fading and offered no capacity under a rate of 3 and 4 C. This improved rate capability of EP–LiF reasonably come from the improved interphase kinetics and reduced overpotential for Li metal utilization, which can be further demonstrated through the voltage profile under various rates in Figure S13 in the Supporting Information. EP–LiF full cell charging and discharging processes called for much suppressed overpotential,

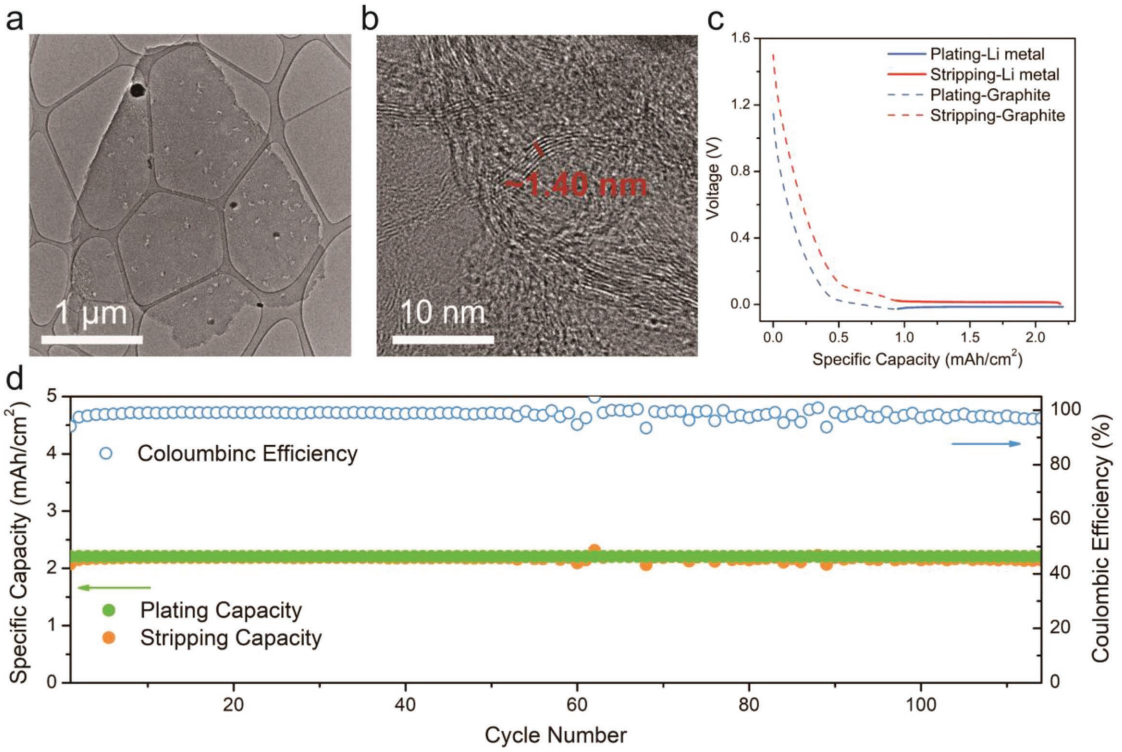

Figure 5. a) TEM image of a carbonized EP sheet. b) High-resolution TEM image showing the graphitic structure of the carbonized EP sheet. c) Voltage profile of Li metal plating and stripping process of a carbonized EP/Li cell. d) Coulombic efficiency results of a carbonized EP/Li cell with areal plating capacity about 2.2 mAh cm^{-2}.

and this is consistent with the symmetric cell and impedance data reported above. Notably, EP–LiF/LCO full cell also showed improved cycling stability than Li foil. It can be observed from Figure 4c that capacity for Li foil/LCO cell after coming back to 0.2 C was much lower than that of first cycle and decayed pretty fast. For EP–LiF/LCO cell, the capacity offered after coming back to 0.2 C was comparable to that of first cycle, and decayed at a moderate rate. Later, Li foil and EP–LiF were also paired with sulfur cathodes with areal mass loading of ≈2 mg cm^{-2} in ether-based electrolyte. EP–LiF/S full cell also manifested improved rate capability (Figure S14, Supporting Information). It offered specific capacity of ≈850 mAh g^{-1} (based on sulfur mass) under a rate of 0.2 C, ≈750 mAh g^{-1} under 0.5 C, ≈650 mAh g^{-1} under 1 C, and ≈500 mAh g under 2 C (current density ≈6.7 mA cm^{-2}). Li foil/S cell, on the contrary, provided specific capacity of ≈700 mAh g^{-1} under 0.2 C, ≈600 mAh g^{-1} under 0.5 C, ≈500 mAh g^{-1} under 1 C, and ≈350 mAh g^{-1} under 2 C. The results above further confirmed the capability of EP–LiF as a high performance anode with improved rate capability and cycling stability in a full cell for commercial applications.

Coulombic efficiency is a crucial parameter of an electrode material, which has always been one of the trickiest problems that hinders the Li metal commercialization. For EP–LiF anodes, we tested its Coulombic efficiency simply using a carbonized EP framework as current collector instead of copper. In a typical case, a carbonized EP framework with areal mass around 2.5 mg cm^{-2} was paired with a piece of Li foil in a coil cell. With ≈60 μL of ether-based electrolyte, we used current density of 1 mA cm^{-2} and capacity of 2.2 mAh cm^{-2} to test the Coulombic efficiency of carbonized EP. It can be observed in **Figure 5**d that carbonized EP offers an average Coulombic efficiency ≈99.1% during the 10th to 100th cycle, which is a great improvement comparing to bare Li foil (Figure S15, Supporting Information) and comparable to recently published works.[15,17,43–46] Meanwhile, we tried to further push the areal capacity in carbonate electrolytes and Figure S16a in the Supporting Information shows the results. Under 1 mA cm^{-2} and 4.72 mAh cm^{-2}, carbonized EP offered an average Coulombic efficiency of ≈95.1%. Although this was still away from the commercialization requirement, the results still manifested solid advancement comparing to bare Li foil. Note that copper as current collector was usually 4–5 times heavier than carbonized EP considering the areal mass. This means we could possibly improve the overall energy density of a full battery using carbonized EP instead of copper as current collector, and achieve a better cycling performance at the same time.

We further researched on the possible reasons for this improved efficiency for carbonized EP. On the voltage curves of Li plating onto carbonized EP in both ether (Figure 5c) and carbonate (Figure S16b, Supporting Information) based electrolytes, we can clearly see two regions of Li metal deposition. One with voltage above (dashed line) and the other below (solid line) 0 V versus Li^+/Li. It is known that Li metal has to be plated below 0 V for overpotential is needed to drive the nucleation and charge transfer (solid line region). Meanwhile, the dashed

line part resembles the charging curve of a graphite anode. To further confirm this, we did transmission electron microscopy (TEM) characterization on carbonized EP. Figure 5a shows an image of a carbonized EP flake. Under high resolution TEM image (Figure 5b), a clear layered structure can be observed on the sample with interlayer spacing of ≈0.35 nm, resembling graphite (≈0.34 nm). The layered structure can be observed throughout the whole sheet, and confirmed that the carbonized EP was actually graphitic carbon and can be lithiated itself. Raman pattern (Figure S17, Supporting Information) of carbonized EP has a high intensity D band, indicating the existence of disorder and defects. It has been previously reported using a 3D packed graphite flake as host material for Li metal that can improve Coulombic efficiency due to the entrapment of Li metal inside the 3D graphite ball.[47] A novel crumpled graphene was also reported to be able to stabilize Li metal deposition.[48] We think the carbonized EP here plays a similar role. After the carbonized EP being fully lithiated, Li metal nucleated inside the channel-like structures of carbonized EP, and could be better protected from electrolyte by the lithiated channel walls and the SEI already formed outside the graphitic carbon. As a result, less Li metal was consumed from the reaction with electrolytes, leading to an improved Coulombic efficiency.

In summary, designing a "host" structure to maintain the volume change during cycling has been proved to be an effective method to improve the cycling capability of Li metal anodes. However, interphase engineering is still needed for a 3D Li metal composite anode to further protect the Li metal reside in the "host" framework. In this work, we combined the channel-like structure of a carbonized EP as a Li metal "host" with a Freon-modified, graphitic carbon–protected Li metal/electrolyte interphase to synthesize EP–LiF as a high performance composite anode. EP–LiF maintained a rather stable volume during cycling to minimize SEI cracking, and also successfully suppressed Li dendrite growth. A better cycling performance with reduced overpotential and smooth voltage plateau in symmetric cell, much improved rate capability in full cells with LCO and sulfur cathodes was also achieved. Furthermore, carbonized EP framework showed much improved Coulombic efficiency of 99.1% serving as a light-weight current collector, attributed to its graphitic structure which facilitated Li nucleation and protection. Overall, EP–LiF offers a possible solution for Li metal anode commercialization considering its cheap cost and simple fabrication procedure. With this interesting structure coming from a natural vegetable, it will also inspire further artificial design for not only Li metal anode, but also cathodes like sulfur to realize practical high-energy battery systems in the near future.

Experimental Section

The experimental methods can be found in the Supporting Information.

Supporting Information

Supporting Information is available from the Wiley Online Library or from the author.

Acknowledgements

The work was supported by the Assistant Secretary for Energy Efficiency and Renewable Energy, Office of Vehicle Technologies of the U.S. Department of Energy under the Battery Materials Research (BMR) program and Battery 500 Consortium.

Conflict of Interest

The authors declare no conflict of interest.

Keywords

Coulombic efficiency, host, lithium metal anodes, SEI

Received: October 9, 2018
Revised: November 15, 2018
Published online:

[1] M. Armand, J. M. Tarascon, *Nature* **2008**, *451*, 652.
[2] S. Chu, A. Majumdar, *Nature* **2012**, *488*, 294.
[3] D. Lin, Y. Liu, Y. Cui, *Nat. Nanotechnol.* **2017**, *12*, 194.
[4] S. Chu, Y. Cui, N. Liu, *Nat. Mater.* **2017**, *16*, 16.
[5] Y. Liu, G. Zhou, K. Liu, Y. Cui, *Acc. Chem. Res.* **2017**, *50*, 2895.
[6] D. Lin, Y. Liu, Z. Liang, H.-W. Lee, J. Sun, H. Wang, K. Yan, J. Xie, Y. Cui, *Nat. Nanotechnol.* **2016**, *11*, 626.
[7] Y. Liu, D. Lin, Z. Liang, J. Zhao, K. Yan, Y. Cui, *Nat. Commun.* **2016**, *7*, 10992.
[8] K. Yan, Z. Lu, H.-W. Lee, F. Xiong, P.-C. Hsu, Y. Li, J. Zhao, S. Chu, Y. Cui, *Nat. Energy* **2016**, *1*, 16010.
[9] Z. Liang, D. Lin, J. Zhao, Z. Lu, Y. Liu, C. Liu, Y. Lu, H. Wang, K. Yan, X. Tao, Y. Cui, *Proc. Natl. Acad. Sci. U. S. A.* **2016**, *113*, 2862.
[10] R. Zhang, X. Chen, X. Shen, X.-Q. Zhang, X.-R. Chen, X.-B. Cheng, C. Yan, C.-Z. Zhao, Q. Zhang, *Joule* **2018**, *2*, 764.
[11] H. Wang, D. Lin, Y. Liu, Y. Li, Y. Cui, *Sci. Adv.* **2017**, *3*, e1701301.
[12] D. Lin, J. Zhao, J. Sun, H. Yao, Y. Liu, K. Yan, Y. Cui, *Proc. Natl. Acad. Sci. U. S. A.* **2017**, *114*, 4613.
[13] W. Li, H. Yao, K. Yan, G. Zheng, Z. Liang, Y.-M. Chiang, Y. Cui, *Nat. Commun.* **2015**, *6*, 7436.
[14] F. Ding, W. Xu, G. L. Graff, J. Zhang, M. L. Sushko, X. Chen, Y. Shao, M. H. Engelhard, Z. Nie, J. Xiao, X. Liu, P. V. Sushko, J. Liu, J.-G. Zhang, *J. Am. Chem. Soc.* **2013**, *135*, 4450.
[15] J. Qian, W. A. Henderson, W. Xu, P. Bhattacharya, M. Engelhard, O. Borodin, J.-G. Zhang, *Nat. Commun.* **2015**, *6*, 6362.
[16] L. Suo, Y.-S. Hu, H. Li, M. Armand, L. Chen, *Nat. Commun.* **2013**, *4*, 1481.
[17] X. Fan, L. Chen, X. Ji, T. Deng, S. Hou, J. Chen, J. Zheng, F. Wang, J. Jiang, K. Xu, C. Wang, *Chem* **2018**, *4*, 174.
[18] Q. Pang, X. Liang, A. Shyamsunder, L. F. Nazar, *Joule* **2017**, *1*, 871.
[19] H. Wang, M. Matsui, H. Kuwata, H. Sonoki, Y. Matsuda, X. Shang, Y. Takeda, O. Yamamoto, N. Imanishi, *Nat. Commun.* **2017**, *8*, 15106.
[20] A. C. Kozen, C.-F. Lin, A. J. Pearse, M. A. Schroeder, X. Han, L. Hu, S.-B. Lee, G. W. Rubloff, M. Noked, *ACS Nano* **2015**, *9*, 5884.
[21] Y. Liu, D. Lin, Y. Yuen Pak, K. Liu, J. Xie, H. Dauskardt Reinhold, Y. Cui, *Adv. Mater.* **2017**, *29*, 1605531.
[22] K. Liu, A. Pei, H. R. Lee, B. Kong, N. Liu, D. Lin, Y. Liu, C. Liu, P.-c. Hsu, Z. Bao, Y. Cui, *J. Am. Chem. Soc.* **2017**, *139*, 4815.
[23] W. Liu, W. Li, D. Zhuo, G. Zheng, Z. Lu, K. Liu, Y. Cui, *ACS Cent. Sci.* **2017**, *3*, 135.

[24] X.-B. Cheng, C. Yan, X. Chen, C. Guan, J.-Q. Huang, H.-J. Peng, R. Zhang, S.-T. Yang, Q. Zhang, *Chem* **2017**, *2*, 258.
[25] N. W. Li, Y. Shi, Y. X. Yin, X. X. Zeng, J. Y. Li, C. J. Li, L. J. Wan, R. Wen, Y. G. Guo, *Angew. Chem., Int. Ed.* **2018**, *57*, 1505.
[26] N. W. Li, Y. X. Yin, C. P. Yang, Y. G. Guo, *Adv. Mater.* **2016**, *28*, 1853.
[27] G. Zheng, S. W. Lee, Z. Liang, H.-W. Lee, K. Yan, H. Yao, H. Wang, W. Li, S. Chu, Y. Cui, *Nat. Nanotechnol.* **2014**, *9*, 618.
[28] G. Zheng, C. Wang, A. Pei, J. Lopez, F. Shi, Z. Chen, A. D. Sendek, H.-W. Lee, Z. Lu, H. Schneider, M. M. Safont-Sempere, S. Chu, Z. Bao, Y. Cui, *ACS Energy Lett.* **2016**, *1*, 1247.
[29] A. Puig, I. Perez-Munuera, J. A. Carcel, I. Hernando, J. V. Garcia-Perez, *Food Bioprod. Process.* **2012**, *90*, 624.
[30] B. Li, D. Geng, X. S. Lee, X. Ge, J. Chai, Z. Wang, J. Zhang, Z. Liu, T. S. A. Hor, Y. Zong, *Chem. Commun.* **2015**, *51*, 8841.
[31] Y. Qu, G. Zan, J. Wang, Q. Wu, *J. Mater. Chem. A* **2016**, *4*, 4296.
[32] T. Chen, Y. Tang, Y. Qiao, Z. Liu, W. Guo, J. Song, S. Mu, S. Yu, Y. Zhao, F. Gao, *Sci. Rep.* **2016**, *6*, 23289.
[33] Z. Li, W. Lv, C. Zhang, B. Li, F. Kang, Q.-H. Yang, *Carbon* **2015**, *92*, 11.
[34] Y. Lu, Z. Tu, L. A. Archer, *Nat. Mater.* **2014**, *13*, 961.
[35] S. Shiraishi, K. Kanamura, Z. i. Takehara, *J. Electrochem. Soc.* **1999**, *146*, 1633.
[36] Q. C. Liu, J. J. Xu, S. Yuan, Z. W. Chang, D. Xu, Y. B. Yin, L. Li, H. X. Zhong, Y. S. Jiang, J. M. Yan, X. B. Zhang, *Adv. Mater.* **2015**, *27*, 5241.
[37] X. Q. Zhang, X. B. Cheng, X. Chen, C. Yan, Q. Zhang, *Adv. Funct. Mater.* **2017**, *27*, 1605989.
[38] S. Choudhury, A. Archer Lynden, *Adv. Electron. Mater.* **2016**, *2*, 1500246.
[39] D. Lin, Y. Liu, W. Chen, G. Zhou, K. Liu, B. Dunn, Y. Cui, *Nano Lett.* **2017**, *17*, 3731.
[40] J. Zhao, L. Liao, F. Shi, T. Lei, G. Chen, A. Pei, J. Sun, K. Yan, G. Zhou, J. Xie, C. Liu, Y. Li, Z. Liang, Z. Bao, Y. Cui, *J. Am. Chem. Soc.* **2017**, *139*, 11550.
[41] X.-Q. Zhang, X. Chen, X.-B. Cheng, B.-Q. Li, X. Shen, C. Yan, J.-Q. Huang, Q. Zhang, *Angew. Chem., Int. Ed.* **2018**, *57*, 5301.
[42] Y. Yuan, F. Wu, Y. Bai, Y. Li, G. Chen, Z. Wang, C. Wu, *Energy Storage Mater.* **2019**, *16*, 411.
[43] C. Zhang, S. Liu, G. Li, C. Zhang, X. Liu, J. Luo, *Adv. Mater.* **2018**, *30*, 1801328.
[44] X. Fan, L. Chen, O. Borodin, X. Ji, J. Chen, S. Hou, T. Deng, J. Zheng, C. Yang, S.-C. Liou, K. Amine, K. Xu, C. Wang, *Nat. Nanotechnol.* **2018**, *13*, 715.
[45] L. Suo, W. Xue, M. Gobet, S. G. Greenbaum, C. Wang, Y. Chen, W. Yang, Y. Li, J. Li, *Proc. Natl. Acad. Sci. U. S. A.* **2018**, *115*, 1156.
[46] S. Chen, J. Zheng, L. Yu, X. Ren, M. H. Engelhard, C. Niu, H. Lee, W. Xu, J. Xiao, J. liu, J.-G. Zhang, *Chem* **2018**, *2*, 1548.
[47] Y. Sun, G. Zheng, Z. W. Seh, N. Liu, S. Wang, J. Sun, H. R. Lee, Y. Cui, *Chem* **2016**, *1*, 287.
[48] S. Liu, A. Wang, Q. Li, J. Wu, K. Chiou, J. Huang, J. Luo, *Joule* **2018**, *2*, 184.